Geomechanics and Engineering, *Vol. 43, No. 1 (2025) 1-11*
https://doi.org/10.12989/gae.2025.43.1.001

Numerical analysis using a newly developed 3D finite element procedure - Part I: Stress behavior at the corner of KIX

Seong-Kyu Yun[a], Hyeonsu Yun[b] and Gichun Kang*

Department of Civil Engineering, College of Engineering, Gyeongsang National University, 501 Jinjudae-ro, Jinju, Gyeongsangn,-do 52828, Republic of Korea

(*Received October 13, 2024, Revised September 14, 2025, Accepted September 21, 2025*)

Abstract. The newly developed three-dimensional finite element program was applied to the problem of the stress and deformation of the reclaimed marine deposits for the connecting bridge at the corner of the Kansai International Airport (KIX) fill. The connecting bridge of KIX is supported by the sea friction piles and the abutment on the airport fill. Differential deformation has been expected to occur at the border of the pile foundation and abutment on the reclaimed fill. Then, for the corner of the large reclaimed island, a three-dimensional analysis is strongly required because a stress dispersion with depth for the applied filling load is expected to occur, and one and two-dimensional approaches have a definite limitation to assess the stress and deformation due to reclamation. Stress dispersion was remarkable with depth. The stress concentration effect due to the existence of a deeply compacted sand column in the alluvial clay layer influenced the subsequent deformation of the Pleistocene deposits. Remarkable lateral displacement, as a typical three-dimensional behavior, was observed in association with long-term settlement. It is noteworthy that the in-situ measured settlement is found to be well described with the calculated performance by the developed 3D elasto-viscoplastic finite element program.

Keywords: elasto-viscoplastic constitutive model; Kansai International Airport (KIX); reclaimed marine foundation; stress dispersion

1. Introduction

In Japan, a number of large-scale reclamations have been executed in Osaka Bay in past decades. Kansai International Airport (KIX) is one of them. These reclaimed islands have undergone much difficulty in the ground behavior due to unforeseen occurrences. These problems are caused by the following special features of the seabed in KIX. The modeling of permeability of the Pleistocene sand layer is not easy because of the continuity and the change in thickness in the horizontal direction, as well as the degree of finer contents at the different locations. And the Pleistocene clays deposited in KIX are so-called "quasi-over-consolidated clays" without definite mechanical overconsolidation history (Mimura and Jang 2004). Most of all, one- and two-dimensional approaches have a definite limitation in assessing the stress and deformation due to reclamation. The seabed in KIX was observed to be non-homogeneous and of irregular thickness. So, a three-dimensional consolidation analysis is hence absolutely required (Mimura and Jeon 2011, 2013, Jeon and Mimura 2011, Jeon 2012). Additionally, many researchers have conducted studies on three-dimensional analysis due to various needs, including research on slope stability (Yamaguchi *et al.* 2018, Yang and Liu 2018), the complex interactions between geocells and soil (Song and Tian 2019), analyses of tunnel junctions (Nawel and Salah 2015) and the effects of stress and water pressure on the permeability of fractured rock masses under three-dimensional stress conditions (Sun *et al*. 2018).

For the above-mentioned reasons, Yun (2020a) developed a three-dimensional finite element analysis program using the elasto-viscoplastic constitutive model. This developed three-dimensional program has been validated and demonstrated by comparison with existing two-dimensional studies.

In the next step, stress and deformation analyses of the Pleistocene foundations for group pile-supported elevated bridge were conducted with the developed three-dimensional elasto-viscoplastic finite element program as the first study to apply the developed three-dimensional program (Yun 2020b). Throughout this study, typical three-dimensional effects, such as stress dispersion with depth due to local loading, can be assessed by the newly developed three-dimensional elasto-viscoplastic finite element program.

In this paper, the newly developed three-dimensional numerical analysis program is applied to the problem of the stress and deformation at the corner of the KIX fill where the foundations of the connecting bridge were set, shown as the red area in Fig. 1. For such an area as the corner of the large reclaimed island, a three-dimensional analysis is strongly required because a stress dispersion with depth for

*Corresponding author, Associate Professor
E-mail: gkang@gnu.ac.kr
[a]Research Professor
E-mail: tjdrb330@gnu.ac.kr
[b]Ph.D. Candidate
E-mail: gustn0672@gnu.ac.kr

ISSN: 2005-307X (Print), 2092-6219 (Online)

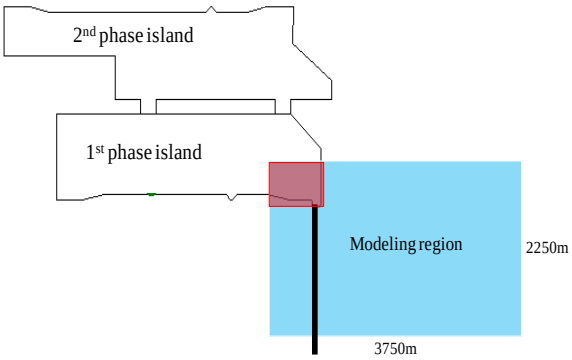

Fig. 1 Northeastern corner of the island with connecting bridge and modeling region

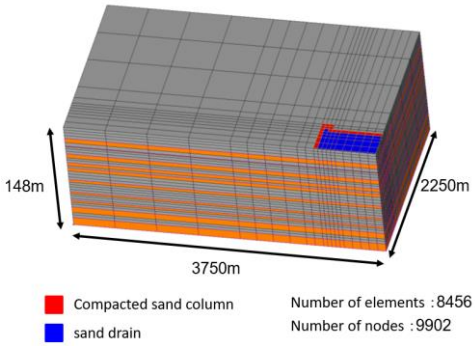

Fig. 2 Modeling for numerical analysis

the applied filling load is expected to occur. One- and two-dimensional approaches have a definite limitation in assessing the stress and deformation due to reclamation. The behavior of the reclaimed airport fill corner should be reasonably explained, considering the effect of stress dispersion and induced settlement and lateral displacement to maintain steady operation of the connecting bridge.

2. Modeling for numerical analysis

2.1 Elasto-viscoplastic model

The elasto-viscoplastic constitutive model proposed by Sekiguchi (1977) was used. In general, the viscoplastic flow rule is shown in Eq. (1).

$$\dot{\varepsilon}_{ij}^{p} = \Lambda \frac{\partial F}{\partial \sigma_{ij}^{'}} \tag{1}$$

in which,

F=Viscoplastic potential

Λ= Proportional constant

Viscoplastic potential F is expressed as Eq. (2).

$$F = \alpha \cdot ln\left[1 + \frac{\dot{v_0} \cdot t}{\alpha} exp\left(\frac{f}{\alpha}\right)\right] = v^{p} \tag{2}$$

n which,

α= Secondary compression index

$\dot{v_o}$ =Volumetric strain rate

f =Function in terms of the effective stress

v^p=Viscoplastic volumetric strain

The concrete form of the model is shown in Eq. (3). The resulting constitutive relations are implemented into the fin ite element analysis procedure through the following increm ental form (Mimura and Sekiguchi 1986)

$$\{\Delta\sigma^{'}\} = [D^{evp}]\{\Delta\varepsilon\} - \{\Delta\sigma^{R}\} \tag{3}$$

in which,

$\{\Delta\sigma^{'}\}$= Effective stress increments

$\{\Delta\varepsilon\}$= Strain increments

$[D^{evp}]$= Elasto- viscoplastic coefficient matrix

$\{\Delta\sigma^{R}\}$= Relaxation stress

Relaxation stress is the increase in stress over time when the strain rate remains constant. The pore water flow is assumed to obey isotropic Darcy's law. It is assumed that the coefficient of permeability, k, depends on the void ratio, e, in the following Eq. (4).

$$k = k_0 \cdot exp\left(\frac{e - e_0}{\lambda_k}\right) \tag{4}$$

in which,

k_o= Initial value of k at $e = e_o$

λ_k= Material constant

Material constant, λ_k, controls the rate of change in permeability subjected to a change in the void ratio. Note that each quadrilateral element consists of four constant strain triangles, and the nodal displacement increments and the element pore water pressure are taken as the primary unknowns of the problem. The finite element equations governing those unknowns are established on the basis of Biot's formulation (Christian 1968, Akai and Tamura 1976), and are solved numerically using the semi-band Gaussian elimination method.

2.2 Conditions of analysis

The foundation model used in the present numerical analysis is shown in Fig. 2. Considering that the calculated performance is free from the boundary effect due to reclamation load, the foundation model is modeled with 3750 m and 2250 m in width, and 148 m in depth. Because the modeled region is wide enough against the loaded area, the effect of the boundary can be ruled out. The total number of the elements and the nodes for the foundation model are 8456 and 9902, respectively. The layers in gray represent the Pleistocene clay layers, and the ones in orange represent the Pleistocene gravel layers. The improved ground regions are shown in red for densely compacted sand columns and blue for sand drain. The names of the individual layers are shown in Fig. 3. Here, Ma denotes the Pleistocene clay layer, and Ds denotes the Pleistocene sand gravel layer.

To reduce calculation time and simplify modeling, the densely compacted sand column and sand drain were not modeled independently. Then, the numerical analysis is performed using the method used in the previous study. For densely compacted sand columns, the settlement reduction coefficient ξ, indicating the reduction in compressibility due

Table 1 Principal soil parameters for the Pleistocene sand gravel layers

	v'	K_0	G_0 (kPa)	k_0 (m/day)	Thickness(m)	name
1	0.33	0.50	13100	2.16E+01	4.5	Ds-1
2	0.33	0.50	13100	1.30E+00	1.0	Ds-2
3	0.33	0.50	13100	1.08E+01	6.0	Ds-3
4	0.33	0.50	13100	3.89E+00	5.0	Ds-4
5	0.33	0.50	13100	3.89E+00	5.0	Ds-5
6	0.33	0.50	13100	2.59E-01	4.0	Ds-6
7	0.33	0.50	13100	8.64E-02	3.0	Ds-7
8	0.33	0.50	13100	2.16E+00	3.0	Ds-8
9	0.33	0.50	13100	2.16E+00	8.5	Ds-9
10	0.33	0.50	13100	6.92E+00	11.0	Ds-10

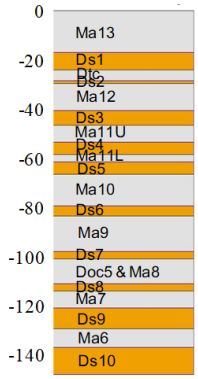

Fig. 3 Name of each layer

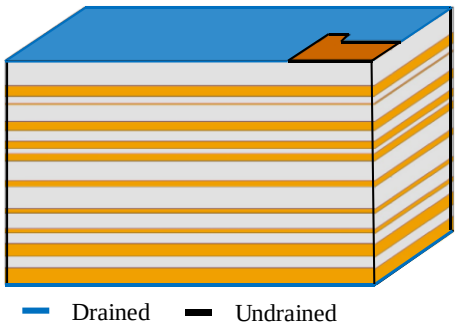

Fig. 4 Drainage boundary conditions

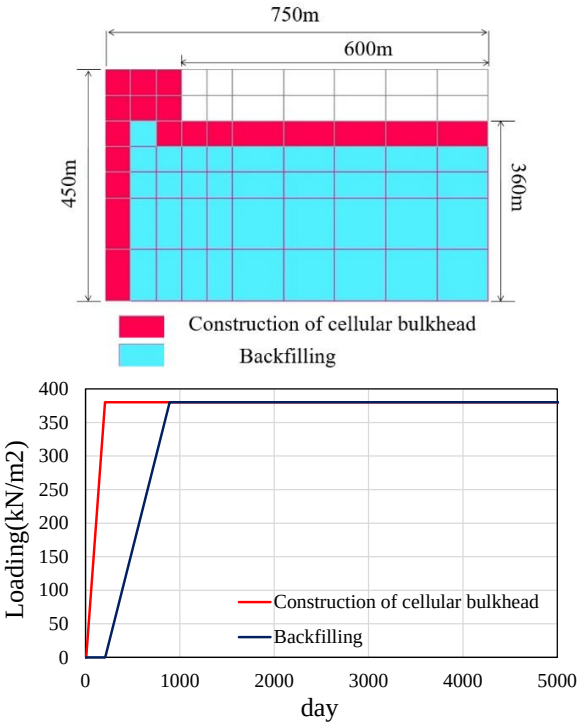

Fig. 5 Loading conditions

to the installation of the sand compact pile, was introduced, as shown in Eq. (5) (Sekiguchi *et al.* 1988). For the sand drain, ten times the permeability coefficient of the Ma13 layer where the sand drain is installed.

$$\xi = 1 - a_s \tag{5}$$

The compression index λ, swelling index κ, and secondary compression index α are reduced as shown in Eq. (6).

$$\begin{aligned} \lambda &\rightarrow \xi \cdot \lambda \\ \kappa &\rightarrow \xi \cdot \kappa \\ \alpha &\rightarrow \xi \cdot \alpha \end{aligned} \tag{6}$$

As far as hydraulic boundary condition is concerned, the side boundary is assumed to be undrained irrespective of materials, while the bottom and top boundaries are assumed to be drained, excluding the loading area (Fig. 4). The loading process is modeled as shown in Fig. 5, reflecting the construction sequence. The cellular bulkhead is constructed as the first stage, shown in red, followed by the airport fill inside the island, shown in blue. Parameters for the sand and clay layers used in the numerical analysis are shown in Tables 1 and 2, respectively.

3. Results and discussions

3.1 Performance of excess pore water pressure

The calculated distribution of excess pore water pressure

Table 2 Principal soil parameters for the Pleistocene clay layers

MTYP	Quasi-OC region				NC region				M	ν'	K_0	p_0 (kPa)	p_c (kPa)	e_0	k_0 (m/day)	λ_k	thickness (m)
	λ_{QOC}	κ_{QOC}	α_{QOC}	$\dot{v}_{0QOC}$ (day-1)	λ	κ	α_{NC}	$\dot{v}_{0NC}$									
1	0.0532	0.0053	6.65E-04	6.65E-07	0.5321	0.0532	6.65E-03	6.65E-06	1.40	0.35	0.540	12.3	25.3	3.00	8.64E-04	0.5321	4.0
2	0.0518	0.0052	7.09E-04	7.09E-07	0.5178	0.0518	7.09E-03	7.09E-06	1.40	0.35	0.540	29.6	39.2	2.65	8.64E-04	0.5178	4.0
3	0.0510	0.0051	7.61E-04	7.61E-07	0.5097	0.0510	7.61E-03	7.61E-06	1.40	0.35	0.540	48.7	57.6	2.35	8.64E-04	0.5097	4.5
4	0.0489	0.0049	8.02E-04	8.02E-07	0.4889	0.0489	8.02E-03	8.02E-06	1.40	0.35	0.540	65.9	80.5	2.05	8.64E-04	0.4889	4.5
5	0.0218	0.0022	5.04E-04	3.76E-07	0.2182	0.0218	5.04E-03	3.76E-06	1.10	0.38	0.607	167.9	268.7	1.16	2.07E-04	0.2182	6.5
6	0.0691	0.0069	1.11E-03	1.83E-07	0.6907	0.0691	1.11E-02	1.83E-06	1.30	0.36	0.561	208.3	312.5	2.10	1.47E-04	0.6907	3.0
7	0.0613	0.0061	1.11E-03	1.83E-07	0.6129	0.0613	1.11E-02	1.83E-06	1.30	0.36	0.561	230.3	345.4	1.76	9.50E-05	0.6129	4.0
8	0.0511	0.0051	9.87E-04	1.62E-07	0.5106	0.0511	9.87E-03	1.62E-06	1.25	0.36	0.572	246.9	370.4	1.59	5.62E-05	0.5106	4.0
9	0.0438	0.0044	8.90E-04	9.51E-07	0.4376	0.0438	8.90E-03	9.51E-06	1.20	0.37	0.583	315.4	425.8	1.46	9.50E-05	0.4376	3.0
10	0.0306	0.0031	6.80E-04	7.27E-07	0.3063	0.0306	6.80E-03	7.27E-06	1.20	0.37	0.583	340.0	459.0	1.25	7.08E-05	0.3063	4.0
11	0.0311	0.0031	6.67E-04	3.15E-06	0.3105	0.0311	6.67E-03	3.15E-05	1.25	0.36	0.572	418.8	565.4	1.33	6.05E-05	0.3105	3.0
12	0.0393	0.0039	9.14E-04	2.55E-07	0.3935	0.0393	9.14E-03	2.55E-06	1.25	0.36	0.572	489.9	612.4	1.15	3.80E-05	0.3935	4.5
13	0.0578	0.0058	1.14E-03	3.17E-07	0.5779	0.0578	1.14E-02	3.17E-06	1.25	0.36	0.572	521.3	651.6	1.54	7.60E-05	0.5779	4.5
14	0.0786	0.0079	1.42E-03	3.97E-07	0.7859	0.0786	1.42E-02	3.97E-06	1.25	0.36	0.572	544.6	680.7	1.76	5.23E-05	0.7859	4.0
15	0.0563	0.0056	1.17E-03	3.18E-07	0.5625	0.0563	1.17E-02	3.18E-06	1.25	0.36	0.572	611.4	764.2	1.40	9.50E-05	0.5625	3.5
16	0.0722	0.0072	1.40E-03	3.79E-07	0.7216	0.0722	1.40E-02	3.79E-06	1.25	0.36	0.572	643.4	804.2	1.58	9.50E-05	0.7216	3.5
17	0.0765	0.0076	1.48E-03	4.02E-07	0.7646	0.0765	1.48E-02	4.02E-06	1.25	0.36	0.572	658.9	823.7	1.58	9.07E-05	0.7646	4.0
18	0.0512	0.0051	1.13E-03	3.07E-07	0.5125	0.0512	1.13E-02	3.07E-06	1.25	0.36	0.572	690.5	863.2	1.27	6.91E-05	0.5125	3.5
19	0.1590	0.0159	2.24E-03	1.58E-06	1.5904	0.1590	2.24E-02	1.58E-05	1.25	0.36	0.572	733.6	880.4	2.55	2.85E-05	1.5904	3.0
20	0.0541	0.0054	1.11E-03	7.86E-07	0.5407	0.0541	1.11E-02	7.86E-06	1.25	0.36	0.572	750.3	900.3	1.43	7.78E-05	0.5407	4.0
21	0.0368	0.0037	8.81E-04	6.23E-07	0.3678	0.0368	8.81E-03	6.23E-06	1.25	0.36	0.572	775.0	930.0	1.09	1.30E-05	0.3678	3.0
22	0.0408	0.0041	9.41E-04	1.36E-06	0.4077	0.0408	9.41E-03	1.36E-05	1.25	0.36	0.572	828.3	994.0	1.17	1.30E-05	0.4077	3.0
23	0.0343	0.0034	8.42E-04	1.22E-06	0.3430	0.0343	8.42E-03	1.22E-05	1.25	0.36	0.572	861.3	1033.6	1.04	3.02E-05	0.3430	4.0
24	0.0442	0.0044	9.91E-04	1.25E-06	0.4415	0.0442	9.91E-03	1.25E-05	1.25	0.36	0.572	941.4	1153.7	1.23	3.54E-05	0.4415	3.5
25	0.0663	0.0066	1.49E-03	1.87E-06	0.6633	0.0663	1.49E-02	1.87E-05	1.25	0.36	0.572	997.4	1196.9	1.23	2.59E-05	0.6633	4.0

with depth is discussed at the most inland point as shown in red in Figs. 6 and 7 shows the calculated result of excess pore water pressure, total stress, effective stress with depth in the ground at 825 days (when the loading is completed), 2000 days, 3000 days, and 4600 days after the start of construction. At 825 days, when the whole filling is completed, in the Holocene clay layer, Ma13, the excess pore water pressure is almost dissipated due to the contribution of the sand drain. In contrast, a large amount of excess pore water pressure is generated in the middle of the Pleistocene deposit from Ma10 to Ma7 because of the poor permeability of Ds6 and Ds7. Then steady dissipation is found to occur with the elapse of time, and at 4600 days, the consolidation is almost completed, although a small amount of excess pore water pressure still remains at Ma9.

Fig. 8 shows the distribution of excess pore water pressure at 825, 2000, 3000, and 4600 days as a contour. Excess pore water pressure remains in large quantities not only in the clay layers but also in the permeable sand gravel layers in the Pleistocene deposits. In particular, large excess pore water pressure is kept in the Pleistocene clay layers, Ma10-Ma7 and DTC-Ma12, as well as sand gravel layers, Ds6-Ds7 and Ds2. This is because these sand gravel layers

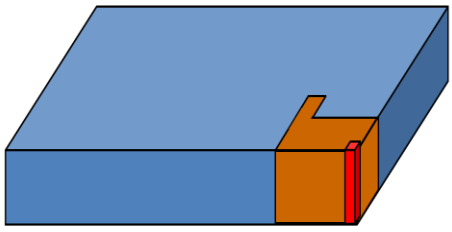

Fig. 6 Location of elements for review

have very poor permeability, which prevents the sufficient propagation of excess pore water pressure. On the other hand, propagation of excess pore water pressure can be seen in the upper and lower Pleistocene deposits, where the permeability of the sand gravel layer is better than that of Ds6 and Ds7.

3.2 Performance of stress

The 3D distribution of effective stress in the ground after 825, 2000, 3000, and 4600 days are shown in Fig. 9. The overall 3D behavior of effective stress in the ground

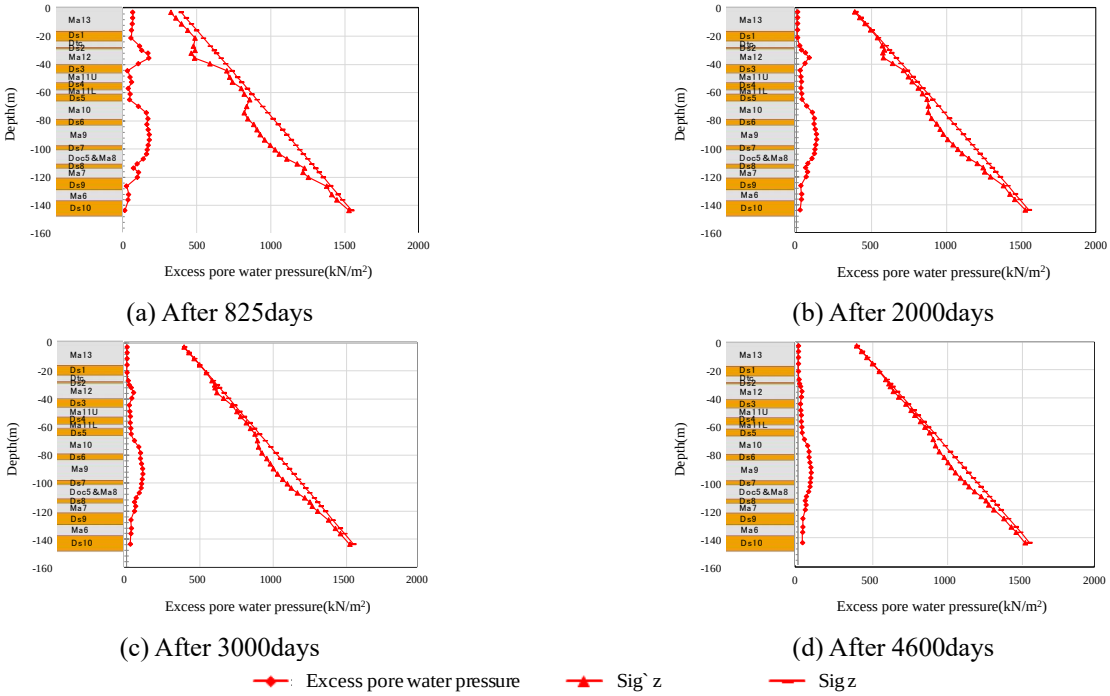

Fig. 7 Calculated result of excess pore water pressure and stress with depth

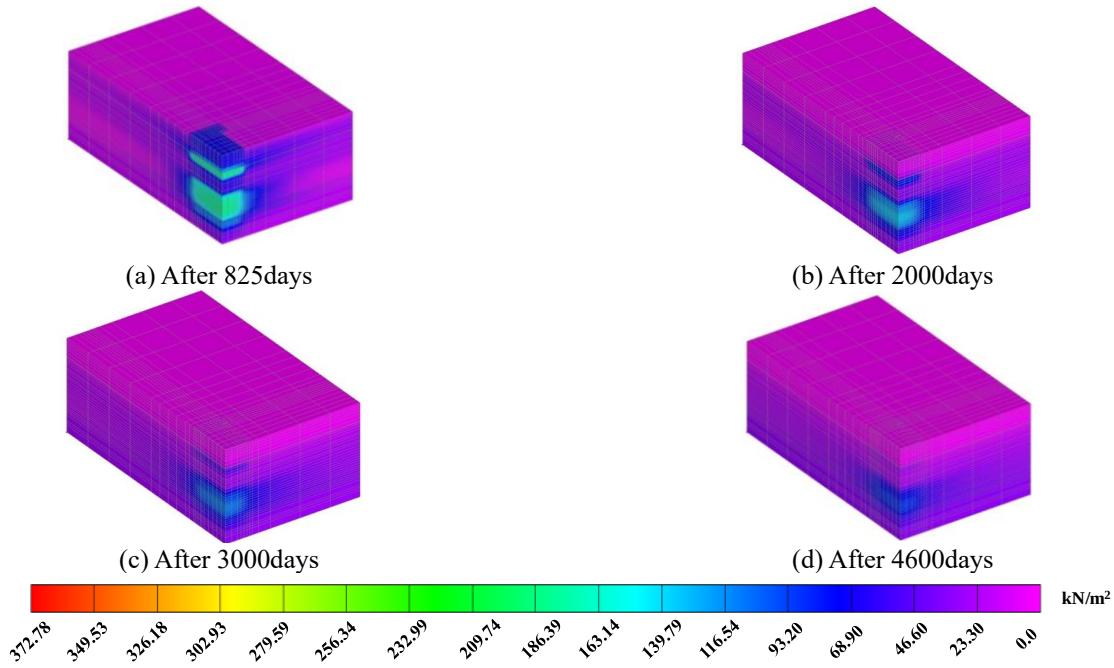

Fig. 8 3D distribution of excess pore water pressure

can be confirmed. Fig. 10 shows the 3D distribution of effective stress, σ`x, σ`y, and σ`z, for the Ma10 layer, as seen from above, which can represent the overall results. The horizontal effective stress showed up wider than vertical effective stress due to stress dispersion by loading. The effect of stress dispersion of σ`x showed up wider than σ`z to the left side, and the effect of stress dispersion of σ`y showed up wider than σ`z to the seaside. According to loading, it was able to see the 3D distribution of vertical effective stress. In particular, the stress reduction effect occurred in the yellow part in Dtc, Ma12, Ma11L, and Ma10 (Fig. 11). In general, the stress reduction effect appears in the upper layers that are more affected by loading. However, Ma10 does not belong to the upper layers, but a stress reduction effect occurred. This is the same reason why large excess pore water pressure was

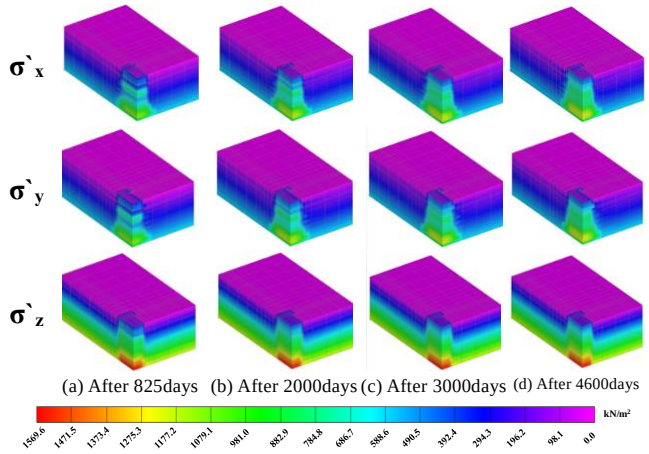

Fig. 9 3D distribution for behavior of effective stress

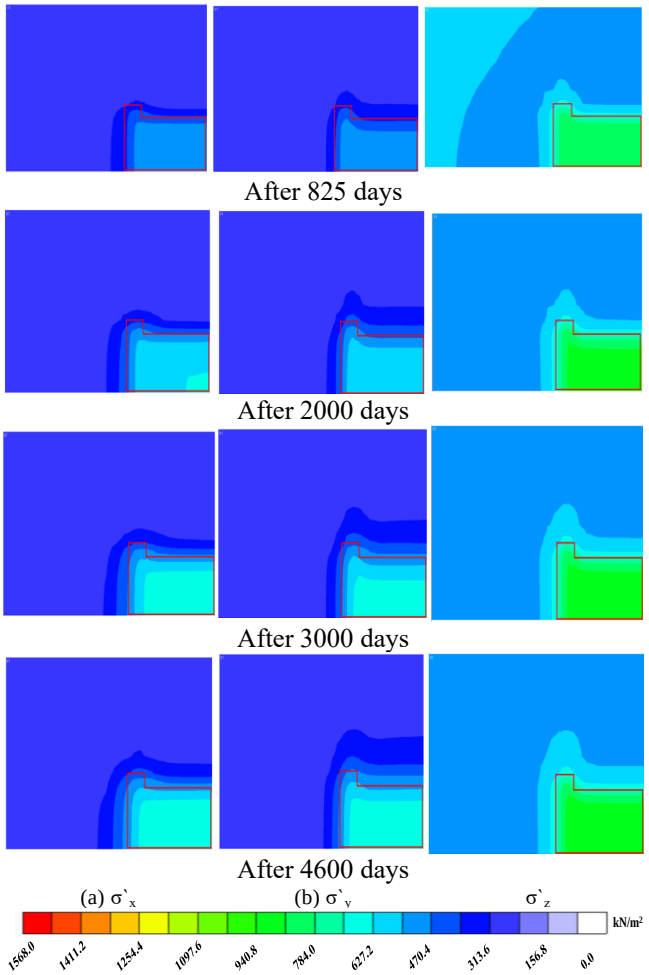

Fig. 10 Distribution of effective stress for Ma 10

generated and dissipated slowly in the Ma10. That is because the thick Pleistocene clay layer Ma10 is sandwiched between the Pleistocene sand gravel layers with poor permeability. The calculated profile of the vertical stress increment, Δσz, with depth due to the reclamation of the airport island is shown in Fig. 12. Three points for discussion are selected, namely the inside of the island (A), the protruded point at the corner (B) and the point along the revetment (C). Here, the applied overburden of the

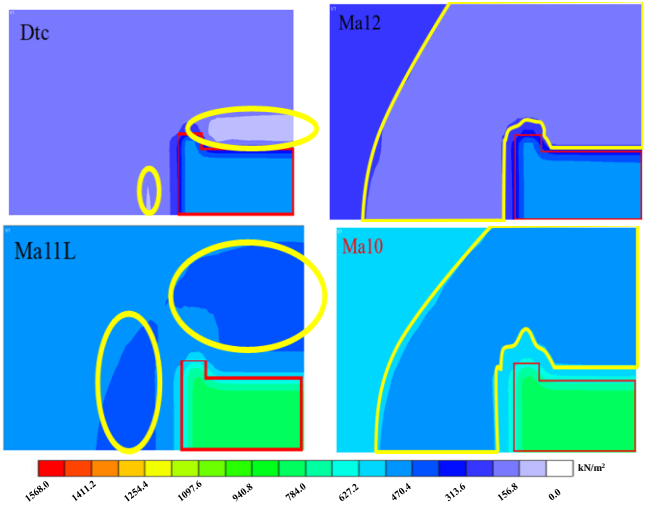

Fig. 11 Layers of the stress reduction effect occurred after 825days

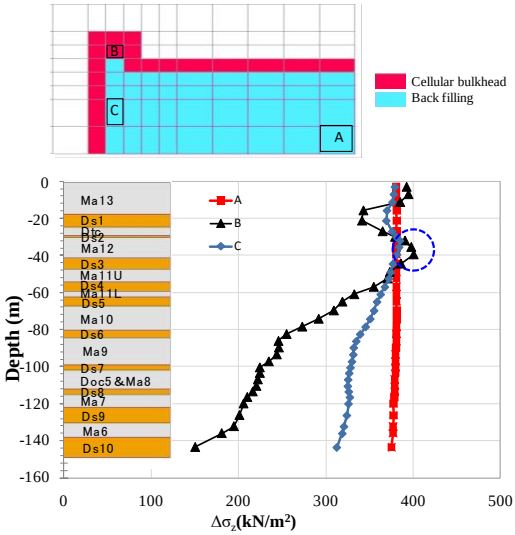

Fig. 12 Calculated depth-vertical stress increment relation for A, B, C

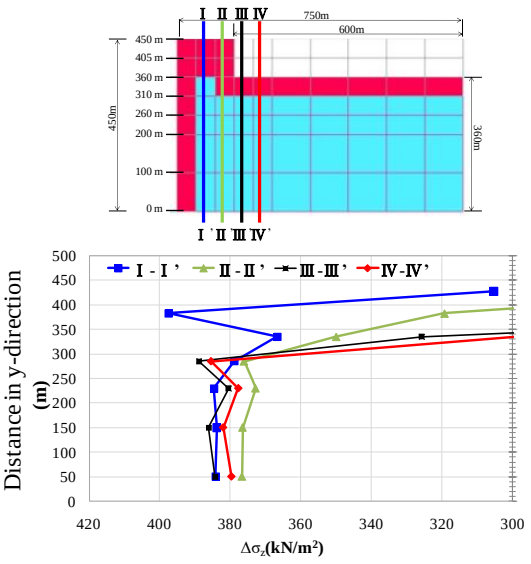

Fig. 13 Calculated vertical stress increment for each line on Ma 12

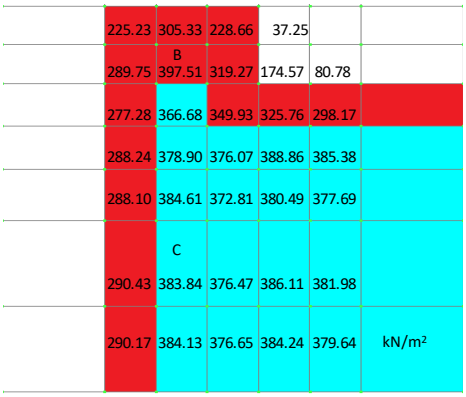

Fig. 14 Calculated profile of the vertical stress increment (Δσz) in Ma 12

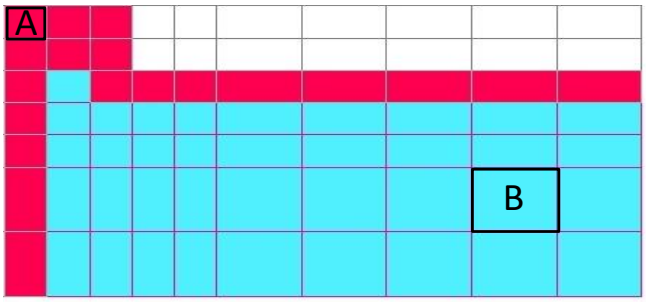

Fig. 15 Calculated point for volumetric strain and deviatoric strain

reclaimed load is 380kN/m2. Almost constant Δσz with depth is found for the inside of the island, (A) without stress dispersion. In contrast, remarkable stress dispersion can be seen for both (B) and (C). Particularly, a serious decrease in Δσz occurs at point (B) due to 3D stress dispersion because (B) is surrounded on three sides by the unloaded area. The point (C) is located in the 2D condition, then, it is natural that Δσz attenuates with depth but not so extremely as the one at point (B). The curious behavior that Δσz once increases followed by decreases with depth at a depth of -32m is found. To explain the mechanism, the horizontal profiles of Δσz of the elements located in the same depth (-32m at Ma 12) are shown in Fig. 13 along the different survey lines I-I', II-II', III-III', and IV-IV'. The alluvial clay deposits in red are improved with densely compacted sand columns, and ones in blue are improved with sand drains. Because the rigidity of the improved alluvial clay deposit with densely compacted sand columns has become higher compared to the one with sand drains, a remarkable stress concentration occurs most clearly along the I-I' line at the border of both areas. Along the II-II' line, a definite protrusion of Δσz does not appear even at the area improved with densely compacted sand columns because the reclamation load is mitigated by facing the unloaded area together with the stress dispersion effect. Figs. 13 and 14 show the calculated profile of the vertical stress increment (Δσz) in Ma12 to understand more easily. The vertical stress increment (Δσz) of point B appears higher than loading (stress concentration), and the vertical stress increment (Δσz) of the edge or corner of the loaded area appears lower than loading (stress dispersion) From these results, a 3D assessment is found to be indispensable, particularly for the edge or corner of the loaded area where the influence of stress dispersion cannot be ignored.

3.3 Performance of 3D dimensional ground deformation

3.3.1 Performance on volumetric strain and deviatoric strain of clay layers

Fig. 16 shows the relation between volumetric strain and deviatoric strain for point A and B of Fig. 15. These figures are able to be obtained from 3D analysis only. The volumetric strain and deviatoric strain were highest at the upper Ma13 and tended to be smaller toward the lower layer. The volumetric strain and deviatoric strain appeared smaller as the depth increased. However, in the exception, the Ma11L was larger than the Ma11U just above it. This is because the Ma11L is located between the Ds4 and Ds5 with good permeability. Comparing the inside of the island (point B) with the outside of the airport (point A), the large volumetric and deviatoric strain appeared inside the airport island. Fig. 17 shows the actual ground deformation after 825, 2000, 3000, and 4600 days. Here, the contour indicates volumetric strain. An hourglass mode was observed, as indicated by the deformed shape of the elements. Hourglass mode is a state of strain, which is free of energy and can emerge in the case of solid and shell elements. Like this figure, it was possible to confirm how the actual ground is deformed at any time through the newly developed 3D numerical analysis.

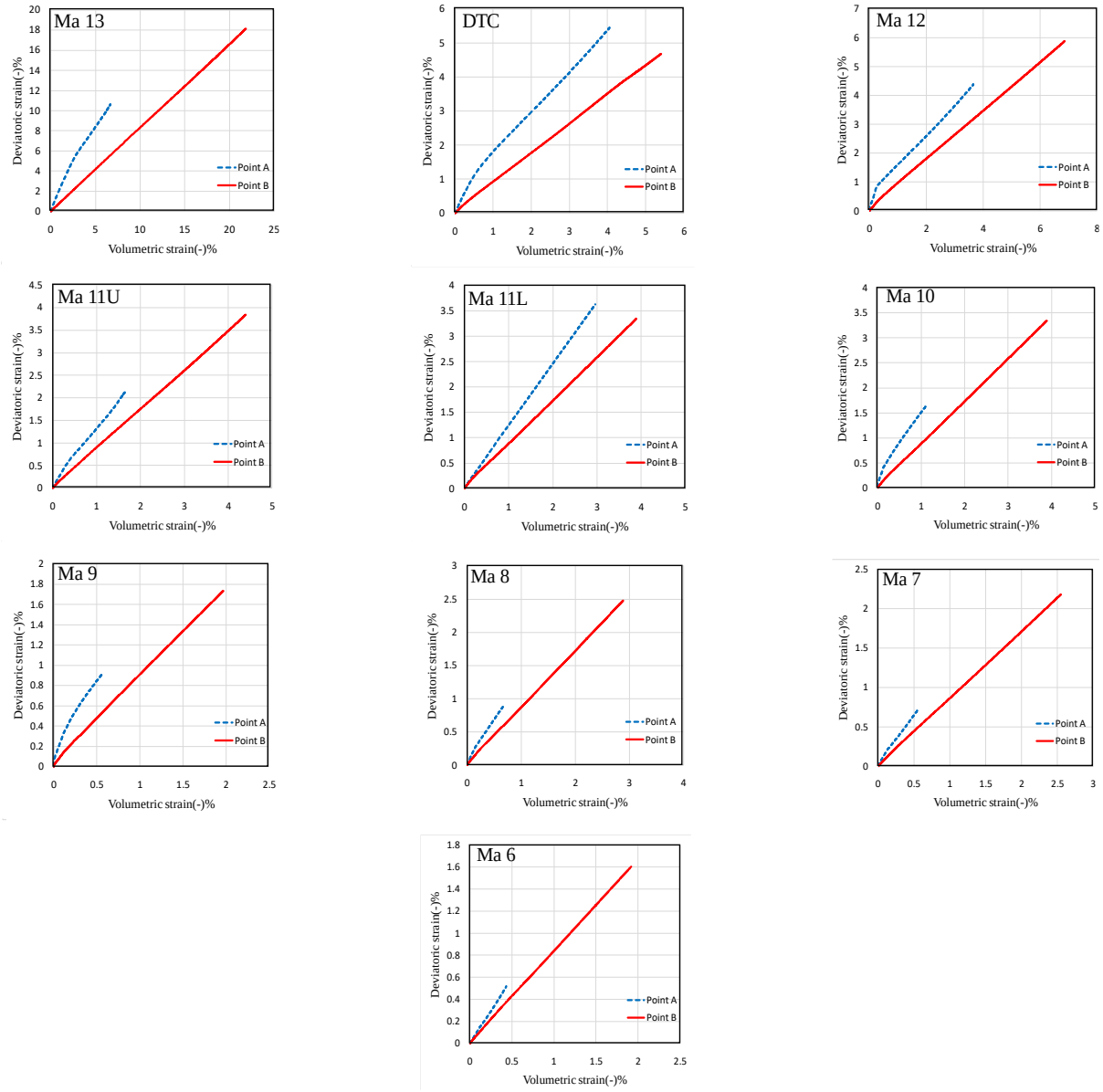

Fig. 16 Relation between volumetric strain and deviatoric strain

3.3.2 Performance of settlement and horizontal displacement

Fig. 18 shows the position of points A-G and X (measured data) for the 3D consideration of settlement and horizontal displacement. Fig. 19 shows the settlement of point X for actual measured data and the results of the present study. It can be confirmed that the result of settlement is well matched with the measured data. Figs. 20-22 show the calculated settlement and horizontal displacement at point A-G. The settlement-time relation is shown in Fig. 20, and Figs. 21 and 22 show horizontal displacement with depth on the 4600th days when displacement occurs the most. In order to consider the results, settlement and horizontal displacement were divided into two groups, respectively. For settlement, one is points A, B, and E, where the compacted sand columns are installed. The other is points C, D, F, and G, where the sand drains are installed. The settlements of points A, B, and E appeared to be less than points C, D, F, and G due to the compression reduction effect of the compacted sand columns. For horizontal displacement in the x direction, Fig. 21 shows the calculated horizontal displacement in the x direction. Depending on the value of the displacement, it can be divided into A, B, C, and D located on the left side(a) and E, F, and G located on the right side(b). The horizontal displacement in the x direction of (a) was larger than (b). In particular, points E, F, and G showed negative displacement in the Holocene marine clay at Ma13. For horizontal displacement in the y direction, Fig. 22 shows the calculated horizontal displacement in the y direction. It can be divided into A, C, F, and E located sea side(a) and B, D, and G located island side(b). The horizontal displacement in y direction of (a) was larger than (b). Points B and C showed negative displacement in the Holocene

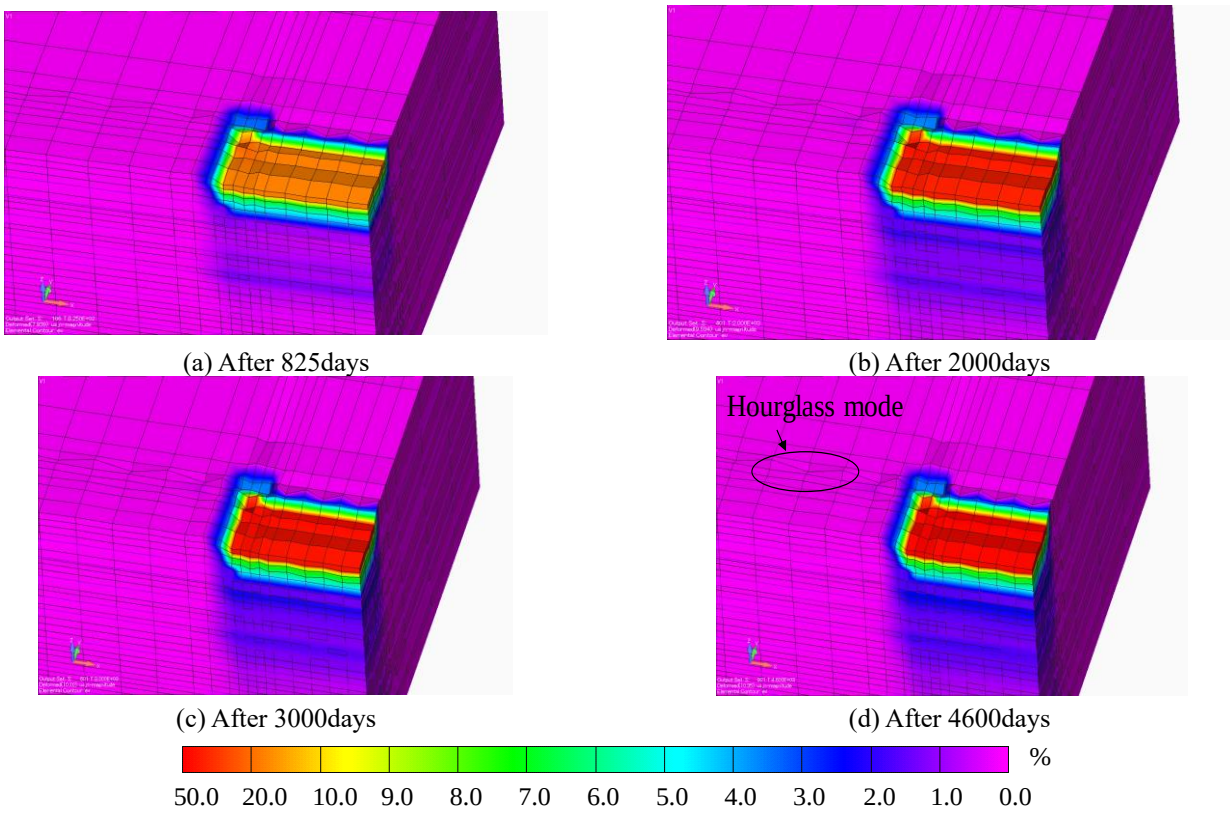

Fig. 17 Actual ground deformation

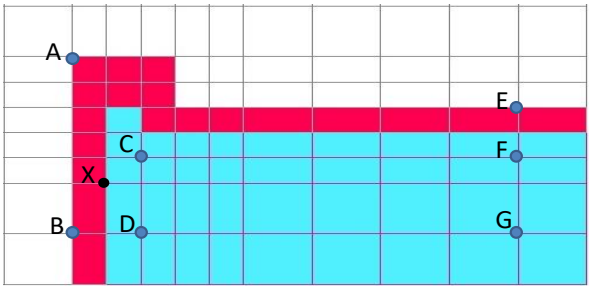

Fig. 18 Measured point for displacement

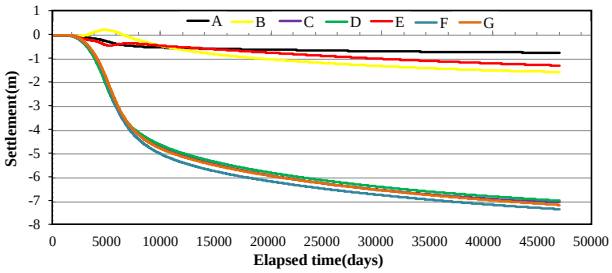

Fig. 20 Result of calculated the settlement

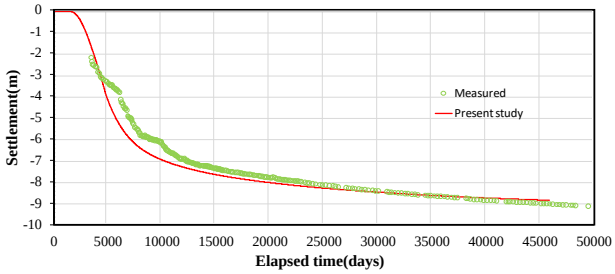

Fig. 19 Comparison of settlement with measured data at point X

marine clay at Ma13. The behavior of the ground for horizontal displacement moved to the seaside in both x and y directions.

4. Conclusions

The newly developed three-dimensional finite element program was applied to the problem of the stress and deformation of the reclaimed marine deposits at the corner of the Kansai International Airport (KIX) fill where the abutment of the connecting bridge has been placed. Densely compacted sand columns have reinforced the soft Holocene clay deposits at the surface of the seabed for the revetments surrounding the airport fill, whereas sand drains have been driven through them for other parts of the reclaimed island. A remarkable difference in stress distribution is expected to appear caused by the stress concentration at the reinforced region where the rigidity of soils definitely increases. For such an area as the corner of the large reclaimed island, a three-dimensional analysis is strongly required because a stress dispersion with depth for the applied filling load is

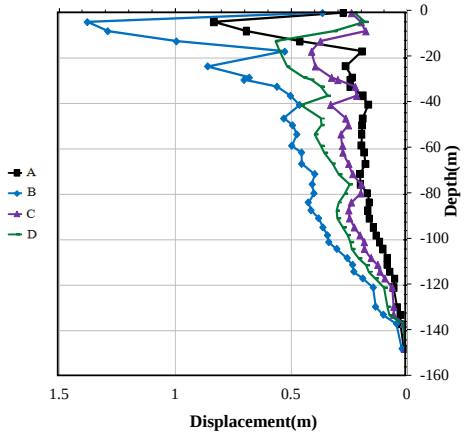

(a) at point A, B, C, D

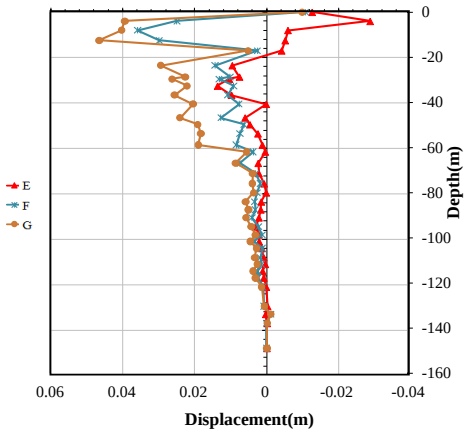

(b) at point E, F, G

Fig. 21 Calculated the horizontal displacement in x direction

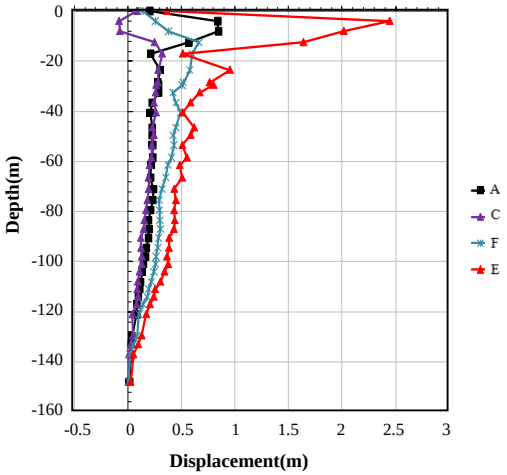

(a) at point A, C, F, E

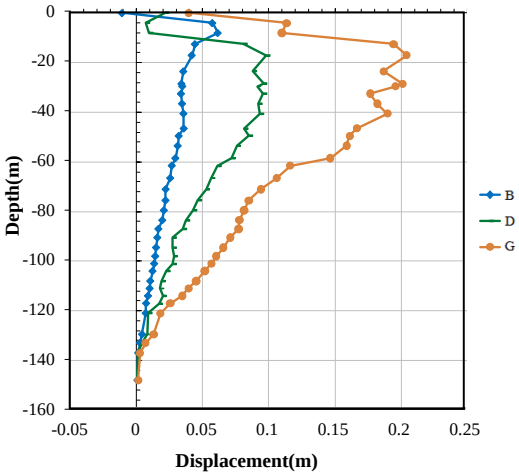

(b) at point B, D, G

Fig. 22 Calculated the horizontal displacement in y direction

expected to occur, and one and two-dimensional approaches have a definite limitation to assess the stress and deformation due to reclamation. It is true that the applied filling load induced excess pore water pressure is generated particularly in the Pleistocene clay layers, but the generated excess pore water pressure is not so large and well dissipated with time because the target area faces the sea on three sides where no filling load is applied to the seabed. Then, the contribution of the excess pore water pressure to the stress and deformation of the reclaimed marine deposits can be ruled out in this particular case. As far as the three-dimensional effect is concerned, serious stress dispersion occurs both horizontally and vertically. In the deep Pleistocene layers, the distribution shape of effective stress becomes far from the shape of the applied filling load, and the affected area becomes wider due to the effect of stress dispersion. At the point close to the end of the island, not all applied filling load is transferred to the deep layer. On the other hand, the vertical stress increment, $\Delta\sigma z$ inside the reclaimed island (and 750 m from the end of the reclaimed island), is almost constant irrespective of depth. It means that the three-dimensional effect in terms of stress dispersion declines with the distance from the end of the reclaimed island. A remarkable gap of stress was found at the boundary between the unimproved region and the one improved with a densely compacted sand column (SCP). In the Pleistocene clay, Ma12 overlain by the SCP improved Holocene clay, stress concentration took place, and the excessive stress was transferred. The calculated performance can well describe this characteristic behavior in the reclaimed marine deposits. The deformation of the reclaimed marine foundation is affected by the three-dimensional stress condition. The calculated performance showed that the settlement of the marine foundations at the end of the airport fill remains small, less than 2 m, and almost converges at 4,600 days from the beginning of construction, while the one inside the island reaches about 7 m. The small amount of settlement at the end of the airport

fill is caused both by the three-dimensional stress dispersion effect and the high rigidity of the reinforced Holocene clay layer, whereas a large settlement occurred inside the island due to the consolidation promoting effect by sand drains. Because it is found that the calculated performance well describes the in-situ measured settlement, the validity of the present three-dimensional assessment is confirmed.

Acknowledgments

This research was supported by Basic Science Research Program through the National Research Foundation of Korea(NRF) funded by the Ministry of Education(No. 2022R1I1A1A01073509).

References

Akai, K. and Tamura, T. (1976), "An application of nonlinear stress-strain relations to multi-dimensional consolidation problems", Annuals DPRI, Kyoto University, 21(B-2), 19-35.

Christian, J.T. (1968), "Undrained stress distribution by numerical method", *J. Soil Mech. Found. Div. ASCE*, **94**(6), 1333-1345. https://doi.org/10.1061/JSFEAQ.0001199.

Jeon, B.G. (2012), "Numerical assessment for long-term behavior of the pleistocene marine foundations due to construction of large-scale offshore airport fill", Ph.D. Dissertation, University of Kyoto, Japan.

Jeon, B.G. and Mimura, M. (2011), "Interactive behavior of the pleistocene reclaimed foundations due to the construction of the adjacent reclamation", Disaster Prev. Res. Inst., Kyoto Univ., **54**, 247-262. http://ci.nii.ac.jp/naid/120003551108.

Mimura, M. and Jang, W.Y. (2004), "Description of time-dependent behavior of quasi-overconsolidated Osaka Pleistocene clays using elasto-viscoplastic finite element analyses", *Soils Found.*, **44**(4), 41-52. https://doi.org/10.3208/sandf.44.4_41.

Mimura, M. and Jeon, B.G. (2011), "Numerical assessment for the behavior of the Pleistocene marine foundations due to construction of the 1st phase Island of Kansai International Airport", *Soils Found.*, **51**(6), 1115-1128. https://doi.org/10.3208/sandf.51.1115.

Mimura, M. and Jeon, B.G. (2013), "Interactive behavior of Pleistocene marine foundation of existing 1st phase island due to construction of 2nd phase island of Kansai International Airport", *Soils Found.*, **53**(3), 375-394. https://doi.org/10.1016/j.sandf.2013.04.001.

Mimura, M. and Sekiguchi, H. (1986), "Bearing capacity and plastic flow of rate-sensitive clay under strip loading", *Bulletin of the Disaster Prevention Research Institute*, **36**(2), 99-111. https://api.semanticscholar.org/CorpusID:67848789.

Nawel, B. and Salah, M. (2015), "Numerical modeling of two parallel tunnels interaction using three-dimensional finite elements method", *Geomech. Eng.*, **9**(6), 775-791. https://doi.org/10.12989/gae.2015.9.6.775.

Sekiguchi, H. (1977), "Rheological characteristics of clays", *Proceedings of the 9th International Conference on Soil Mechanics and Foundation Engineering*, Tokyo, July

Sekiguchi, H., Shibata, T., Mimura, M. and Sumikura, K. (1988), "Behavior of the seawall and bridge abutment at the edge of an offshore airport fill", *Annuals Disaster Prevention Research Institute*, **31**(2), 123-145.

Song, F. and Tian, Y. (2019), "Three-dimensional numerical modelling of geocell reinforced soils and its practical application", *Geomech. Eng.*, **17**(1), 1-9. https://doi.org/10.12989/gae.2019.17.1.001.

Sun, W., Xue, Y., Yin, L. and Zhang, J. (2019), "Experimental study on seepage characteristics of large size rock specimens under three-dimensional stress", *Geomech. Eng.*, **18**(6), 567-574. https://doi.org/10.12989/gae.2019.18.6.567.

Yamaguchi, K., Takeuchi, N. and Hamasaki, E. (2018), "Three-dimensional simplified slope stability analysis by hybrid-type penalty method", *Geomech. Eng.*, **15**(4), 947-955. https://doi.org/10.12989/gae.2018.15.4.947.

Yang, X.L. and Liu, Z.A. (2018), "Reliability analysis of three-dimensional rock slope", *Geomech. Eng.*, **15**(6), 1183-1191. https://doi.org/10.12989/gae.2018.15.6.1183.

Yun, S.K. (2020a), "Demonstration of developed numerical procedure to describe 3-dimensional long-term behavior of the Pleistocene marine foundations", *J. Korean Geotech. Soc.*, **36**(7), 5-14. https://doi.org/10.7843/kgs.2020.36.7.5.

Yun, S.K. (2020b), "Development of the Numerical Procedure to Describe multi-dimensional Behavior of the alternating Pleistocene Foundations", Ph.D. Dissertation, University of Kyoto, Japan.

IC